Supplement of Atmos. Chem. Phys., 20, 6243–6257, 2020
https://doi.org/10.5194/acp-20-6243-2020-supplement

Atmospheric Chemistry and Physics
Open Access
EGU

Supplement of

Seawater analysis by ambient mass-spectrometry-based seaomics

Nicolás Zabalegui et al.

Correspondence to: María Eugenia Monge (maria.monge@cibion.conicet.gov.ar)

Table S1. Information related to sampling conditions, sample salinity, pH and temperature.

Collection Date (dd/mm/yyyy)	Local Time (hh:mm)	Observations	Type of Sample						Sample ID
			ULW			SML			
			Salinity [psU]	pH	Temp [°C]	Salinity [psU]	pH	Temp [°C]	
18/9/2017	11:35-12:00	Premature discontinuation of sampling	34.1	8.14	25.0	-	-	-	ULW GP1 - SML GP1
20/9/2017	08:32-09:54 (ULW sampling: 09:43)	Sampling with three glass plates manually – At later sampling time: increased occurrence of slick and foam	36.3	8.12	26.7	36.2	8.11	26.7	ULW GP2 - SML GP2
26/9/2017	11:00-12:00 (sampling time for 45 min)	Catamaran	36.2	8.04	26.1	36.4	8.05	26.1	ULW CAT3 - SML CAT3
27/9/2017	8:50-10:03	Catamaran	36.2	7.91	27.0	36.0	7.97	26.7	ULW CAT4 - SML CAT4
2/10/2017	08:30-09:30	Very windy, ULW sampling was performed on a different place than SML sampling because of the drift	36.0	8.17	20.9	36.5	8.26	20.9	ULW GP5
2/10/2017	08:30-09:30	Catamaran sampling was interrupted because of the drift, after changing the sampling position sampling was continued	35.9	8.15	22.7	36.1	8.12	23.9	ULW CAT5- SML CAT5
3/10/2017	08:15-09:35	-	36.2	8.17	23.5	36.3	8.18	22.4	ULW CAT6 - SML CAT6
6/10/2017	08:04-08:34 (ULW sampling and 1 L SML) 09:02 -09:47 (2 L SML)	Firstly, premature discontinuation because of seasickness. Went out a second time for more SML sampling	36.3	8.21	23.7	36.6	8.20	20.7	ULW GP7
7/10/2017	09:22-09:41 (ULW sampling) 09:45-10:35 (SML sampling)	Smaller and higher waves in change	36.4	8.22	21.8	36.7	8.22	21.2	ULW GP8 - SML GP8
7/10/2017	09:17-10:46	-	36.5	8.21	22.4	36.7	8.19	24.5	ULW CAT8 - SML CAT8
9/10/2017	08:30-9:17 (08:30-08:37 ULW sampling; 08:40-09:12 SML sampling)	Windy - only manual sampling (no use of the CAT)	36.4	8.13	23.6	36.6	8.19	21.5	ULW GP9 - SML GP9
10/10/2017	08:30-09:30 (09:30-08:40 ULW sampling) 08:45-09:30 SML sampling	Windy up to very windy with long waves (but sampling conditions were okay)	36.3	8.18	22.4	36.4	8.19	21.7	ULW GP10 - SML GP10

Table S2. Chemical standard mixtures used for the analytical method development and for system suitability check prepared in ultrapure water.

Mix	Compound	Exact mass	Concentration/µgmL^{-1}
Amino acids (10 mg/mL)	Gly	75.0320	4
	Ala	89.0477	
	GABA	103.0633	
	Ser	105.0426	
	Pro	115.0633	
	Val	117.0790	
	Thr	119.0582	
	Ile	131.0946	
	Leu	131.0946	
	Asn	132.0535	
	Asp	133.0375	
	Gln	146.0691	
	Glu	147.0532	
	Met	149.0510	
	His	155.0695	
	Phe	165.0790	
	Arg	174.1117	
	Trp	204.0899	
Sugars (100 mg/mL)	Xylose	150.0528	4
	Fucose	164.0685	
	Galactosamine	179.0794	
	Glucose	180.0364	
	Mannitol	182.0790	
Lipids (MeOH:H_2O, 3:1 v/v)	Decanoic Acid	172.1463	0.23
	Dodecanoic acid	200.1776	0.06
	Octadecanoic acid	284.2715	0.09
	Eicosanoic acid	312.3028	0.25
	Docosanoic acid	340.3341	0.10

Table S3. List of compounds (M1 and M2) and associated *m/z* values of adduct ions utilized for the time-of flight calibration with the DART source operated in transmission mode geometry.

Adduct Ion	M1	M2	*m/z*
$[M1-H]^-$	2-Cyanoguanidine	-	83.0363
$[M1-H]^-$	Maleic acid	-	115.0037
$[M1-H]^-$	Mercaptosuccinic acid	-	148.9914
$[M1-H]^-$	2-Amino-4,5-dimethoxybenzoic acid	-	196.0615
$[M1-H]^-$	Lacosamide	-	249.1245
$[M1+M2-H]^-$	2-Cyanoguanidine	2-Amino-4,5-dimethoxybenzoic acid	280.1051
$[M1-H]^-$	Enalapril	-	375.1925
$[M1-H]^-$	Flecainide	-	413.1305
$[M1+Cl]^-$	Flecainide	-	449.1072
$[M1+M2-H]^-$	Flecainide	Maleic acid	529.1415
$[M1+M2-H]^-$	Flecainide	2-Amino-4,5-dimethoxybenzoic acid	610.1993
$[M1+M2-H]^-$	Enalapril	Lacosamide	625.3243
$[2M1-H]^-$	Enalapril	-	751.3923
$[M1+M2-H]^-$	Flecainide	Enalapril	789.3303

Table S4. Fold change analysis for discriminant features. Wilcoxon Paired Signed Rank Test was used to compare SML with ULW samples. Features with p <0.05 are highlighted in bold; enrichment in SML is highlighted in red and in ULW in green.

Feature Code	Fold Change SML/ULW											Trend
	GP1	GP2	CAT3	CAT4	GP8	GP9	GP10	CAT5	CAT6	CAT8	Median of paired SML/ ULW	
4	0.9	0.9	1.1	0.9	0.9	0.8	1.1	0.9	1.1	1.1	0.9	↓
5	1	1.2	0.9	0.8	1.2	0.8	1.5	1.1	1.5	1.4	1.2	↑
17	**1.2**	**1.1**	**1.3**	**1.2**	**1**	**1.1**	**1.5**	**1**	**1.5**	**1.3**	**1.2**	↑
21	0.9	1.1	0.4	2.3	0.8	1.1	1.4	1.4	1.4	1.1	1.1	↑
25	**0.9**	**0.9**	**0.7**	**0.4**	**0.9**	**0.5**	**0.8**	**0.7**	**1.2**	**1.1**	**0.9**	↓
28	1.4	1.3	0.6	0.8	1	0.9	1.2	0.9	1.3	1	1.1	↑
31	**1.2**	**1.3**	**1.2**	**0.9**	**1.1**	**1.1**	**1.1**	**1.1**	**1.1**	**1.1**	**1.1**	↑
33	**1.5**	**1.2**	**1**	**1.1**	**1.1**	**1.2**	**1.2**	**1.2**	**1**	**1**	**1.2**	↑
34	1.1	1	0.5	2.5	0.7	0.9	1.1	1	1.4	1.1	1.1	↑
43	1	1.7	1	0.8	0.9	1	0.7	0.9	0.8	0.8	0.9	↓
49	**0.7**	**0.6**	**1.1**	**0.6**	**0.9**	**0.6**	**0.7**	**0.6**	**1.1**	**1**	**0.7**	↓

Table S5. Putative identification of features with loading values associated to PC2 higher than 0.25 (Fig. S8 A and B). Normalized average intensity values are indicated for SML samples analyzed with both the lab-to-the-field approach and TM-DART-QTOF-MS.

Feature #	Feature (*m/z*)	Putative ID	No SOA formation			SOA formation	
			CAT3	CAT4	CAT6	CAT8	GP10
13	**439.3164**	-	1.4	1.2	1.7	2.3	1.9
28	**639.4312**	**Boron-containing organic compound**	7.0	6.6	7.3	11.0	8.0
29	**639.5013**	**Boron-containing organic compound**	6.6	6.8	6.9	8.5	8.2
32	**667.4628**	**Boron-containing organic compound**	3.2	3.0	3.2	4.5	3.6
33	**667.5346**	**Boron-containing organic compound**	139.8	128.8	131.8	160.2	160.4
38	**698.5176**	-	9.8	9.5	11.0	12.3	13.7
42	**726.5480**	-	14.1	14.1	16.1	17.3	19.1

Figure S1. Irradiation spectrum measured at the quartz reactor illuminated by UV and pen ray lamps

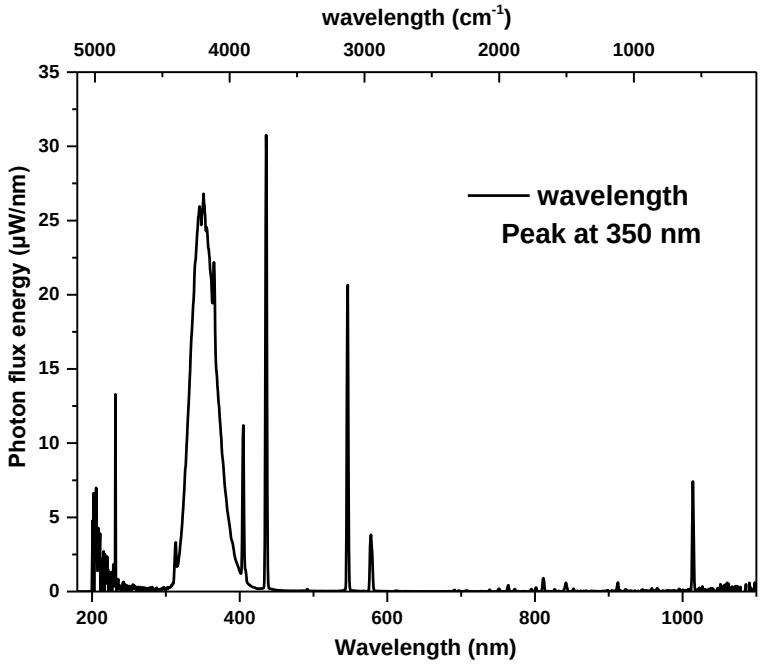

Figure S2: Schematic setup of the PAM chamber (OFR_{254}) system deployed in this marine air photochemistry field study. Solid lines show the flow chart for particle formation potency from the sea surface microlayer (SML) interfacial photochemical production.

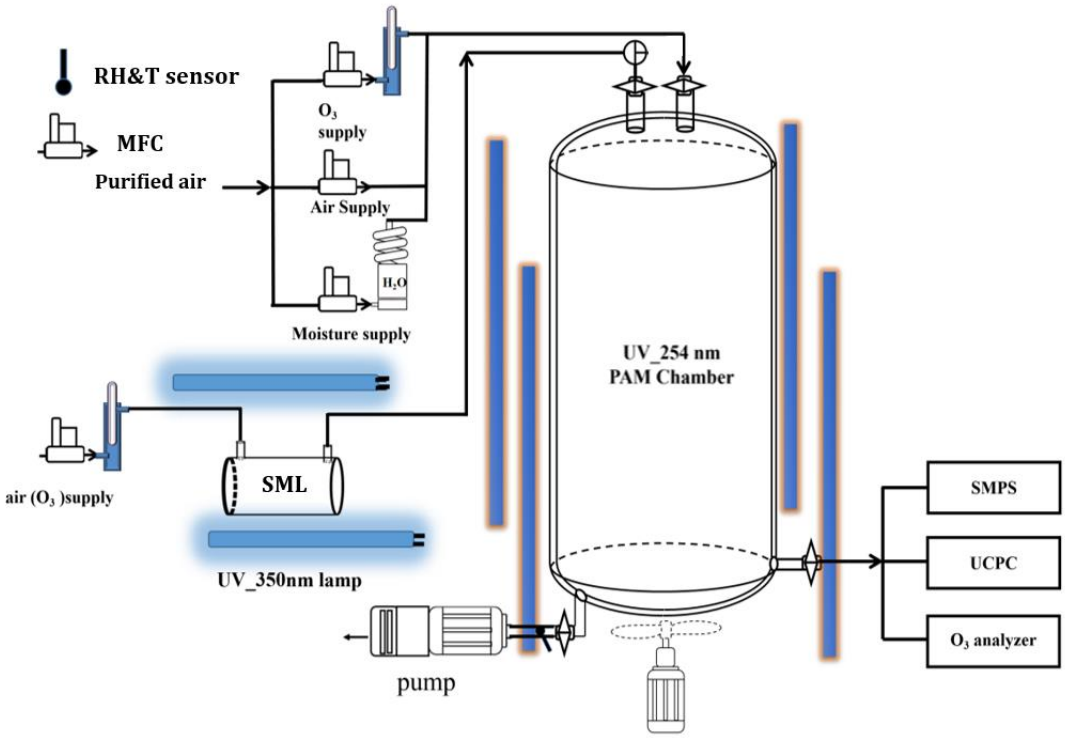

Supporting Text 1. Oxidation flow reactor (OFR)

The Potential Aerosol Mass (PAM) oxidation flow reactor (OFR) is now commonly used in atmospheric chemistry to study the aging of a given air mass, and to investigate aerosol formation and aging. Operational principles and applications of the OFR have been described in previous works (Palm et al., 2016; Saukko et al., 2012). Briefly, the OFR in this study is equipped with 254 nm UV light, hereafter named as OFR_{254}. The OFR_{254} (GoPAM 2) is different from general Aerodyne OFR, which is made completely of coated aluminum walls with the UV lamps inserted inside the chamber (Kang et al., 2011; Li et al., 2015). This OFR_{254} consists of a vertical cylindrical quartz tube (length: 95 cm, ID: 12.4 cm) with an internal volume of approximately 11.5 L. Two controllable low-pressure mercury UVA lamps (Philips, Inc.) with characteristic output spectra at 254 nm are vertically mounted surrounding the high-transmission tube. The tube and lamps are sealed in an aluminum box, with continuous ventilation to prevent heating. Two inlets allow introducing the auxiliary gases (e.g., N_2/air, moisture, O_3, etc.) and ambient/sample air (e.g., SO_2, VOCs, etc), separately. A static mixer at the top of the reactor enables uniform mixing of the auxiliary gases and sample air before flowing through the OFR_{254}. Residence time (RT) inside this reactor is 137 s for a laminar flow (Reynold's number ~57.1<2000) at 5 LPM. OH radicals in the OFR_{254} can be produced through photolysis of O_3 and further reaction of singlet oxygen (O^1D) with moisture. Detailed pathways for OH radical production are presented below:

$$O_3 \xrightarrow{hv(254\,nm)} O^1D + O_2 \qquad \text{R1}$$

$$O^1D + H_2O \rightarrow 2OH \qquad \text{R2}$$

The OFR_{254} requires the addition of an external O_3 source. Initial O_3 concentration, water vapor density, UV light intensity and RT strongly influence the chemistry in the OFR. The complicated radical chemistry in the OFR_{254} (e.g., OH radical dominated oxidation pathways over O_3, HO_2, and RO_2 reactions) can be simply characterized as OH exposure (OH_{exp}), which works as a vital parameter to denote the oxidation level of the sample. OH exposure is defined as an integration of the reactive OH radical density with residence time in the OFR. Simulations confirm the complex correlation of OH_{exp} with many variables including external total OH reactivity ($OHR_{ext}=\Sigma k_i \times [R_i]$, where k_i and $[R_i]$ are the reaction kinetic constant with OH and the concentration of the OH-consuming reactant in the system), humidity, RT, UV light intensity, and initial O_3 or/and static endpoint O_3. Some non-linear mathematical functions containing all these variables have been proposed to estimate the OH_{exp} (Aerodyne OHexp estimator) (Peng et al., 2015). To be convenient, most studies apply some reactive tracers (e.g., SO_2, CO,

target VOCs) to measure or to constrain the OH_{exp} by measuring their first-order decay in OFR via Equation 1:

$$OH_{\exp} = \frac{1}{k}\ln(\frac{C_0}{C}) \quad [1]$$

where *k* is the second-order rate constant with OH radical in gas phase, C_0 and C are initial and final concentrations of the chemical tracer. We followed the mathematical models suggested by Li et al. (2015) and Peng et al. (2015) to retrieve the operational function for our OFR_{254}. OHexp was explored over a wide range of conditions in the laboratory, and the OH_{exp} estimation functions were retrieved and shown in Equation 2 and 3 below, corresponding to one and two UV lamps full-power irradiation.

$$\log(OH\exp) = 1.732 + 0.79292\times\log(RH) + 0.023076\times\log(RH)^2 + 0.978\times\log(RT) - \log\left\{1+\exp\left[\frac{-1.22-\log(O_3/OHR)}{0.421}\right]\right\} \quad [2]$$

$$\log(OH\exp) = 1.991 + 0.79292\times\log(RH) + 0.023076\times\log(RH)^2 + 0.978\times\log(RT) - \log\left\{1+\exp\left[\frac{-1.22-\log(O_3/OHR)}{0.41}\right]\right\} \quad [3]$$

The OH_{exp} estimated based on equations 2 and 3 was compared against the OHexp measured from the SO_2 decay, and the results are shown in Figure S3, where it is clear that the estimated OHexp data points are within a factor of 1 from the measured OH_{exp}. OH_{exp} can be converted to equivalent days of OH radicals initiated atmospheric aging by dividing by a 24 h average ambient concentration of 1.5×10^6 molec cm^{-3} OH. It should be noted that in air with high oxidation capacity, like remote oceanic areas, average OH radical density can be up to 9×10^6 molec cm^{-3}(Carpenter et al., 2010). Therefore, to account for the extreme levels of OH radicals, OH_{exp} in this campaign was stepped over a wide range by adjusting light intensity and also external ozone concentration.

Figure S3. Comparison of OH exposure (OH_{exp}) estimated from Equations 2 and 3 vs. the measured OH_{exp} results. 1:1, 1:2, 2:1, 1:4, and 4:1 lines are shown to facilitate the comparison.

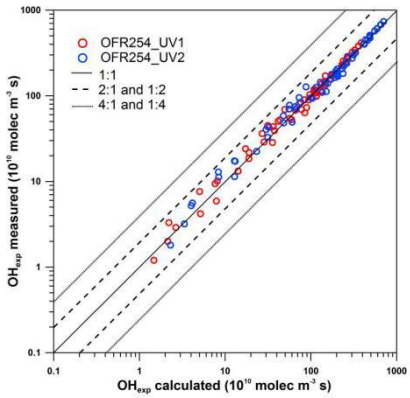

Figure S4: Experimental design for depositing samples in the mesh.

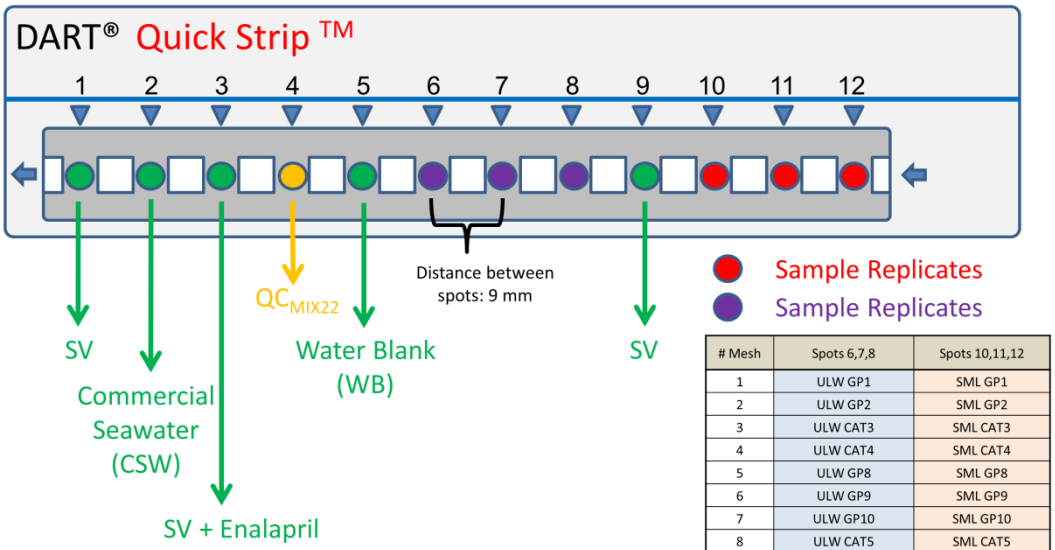

# Mesh	Spots 6,7,8	Spots 10,11,12
1	ULW GP1	SML GP1
2	ULW GP2	SML GP2
3	ULW CAT3	SML CAT3
4	ULW CAT4	SML CAT4
5	ULW GP8	SML GP8
6	ULW GP9	SML GP9
7	ULW GP10	SML GP10
8	ULW CAT5	SML CAT5
9	ULW CAT6	SML CAT6
10	ULW CAT8	SML CAT8
11	ULW GP5	ULW GP7
12	QC_{ALL}	-

Figure S5: t-SNE plot for replicate SML and ULW samples.

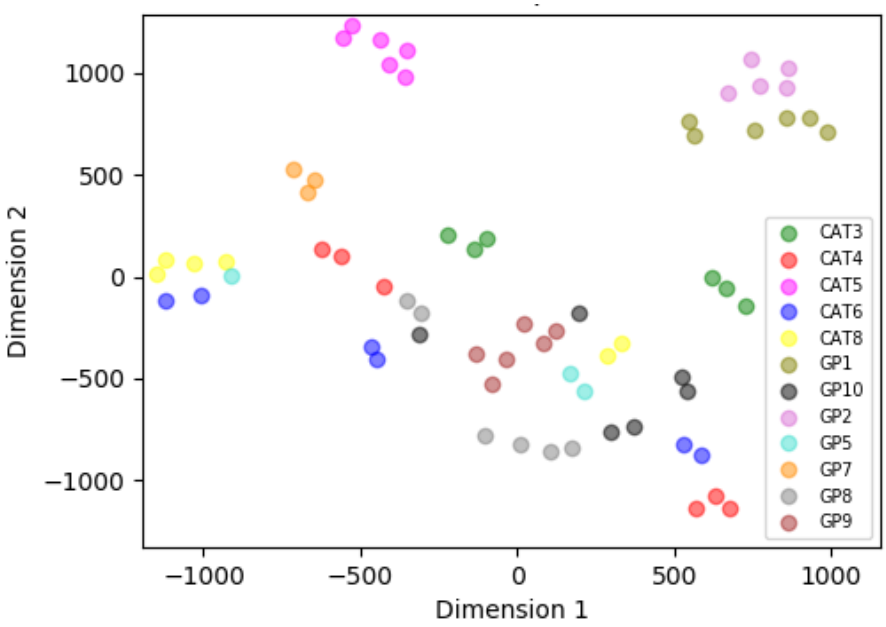

Figure S6. TM-DART-QTOF-MS continuum spectra of discriminant features. Peaks from the isotopic pattern are indicated with arrows and feature codes are indicated between brackets (Table 1).

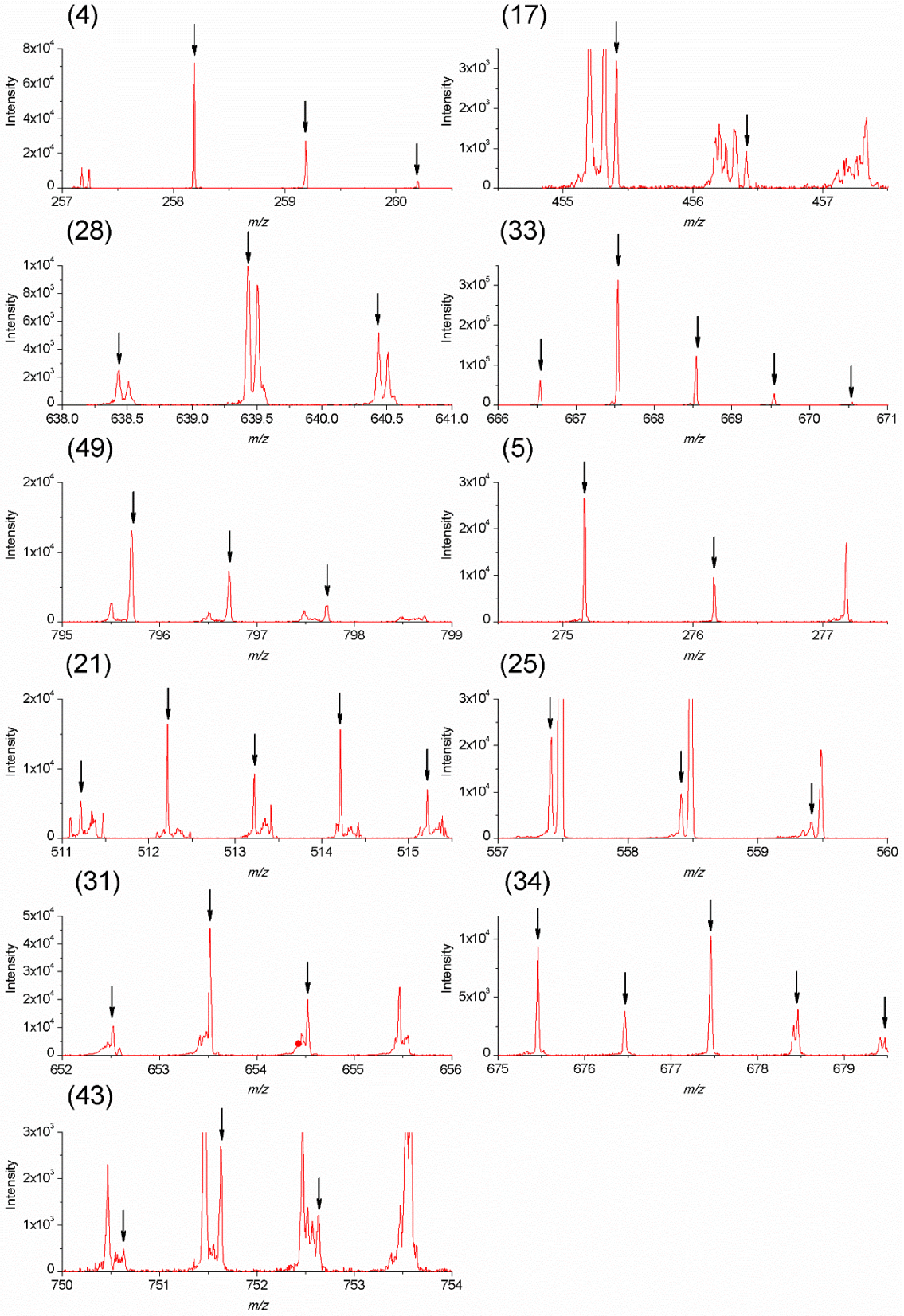

Figure S7: (a) Mass spectrum of a 0.32 mM 4-bromo-phenol solution in acetonitrile obtained using TM-DART-QTOF-MS. (b) Tandem MS spectrum for the precursor ion at *m/z* 170.9456 using 10 V in the collision cell for fragmentation and a quadrupole selection window of 1 Da. (c) Mass spectrum of a saturated acetonitrile solution with KBr and 2 mM phenol obtained using TM-DART-QTOF-MS.

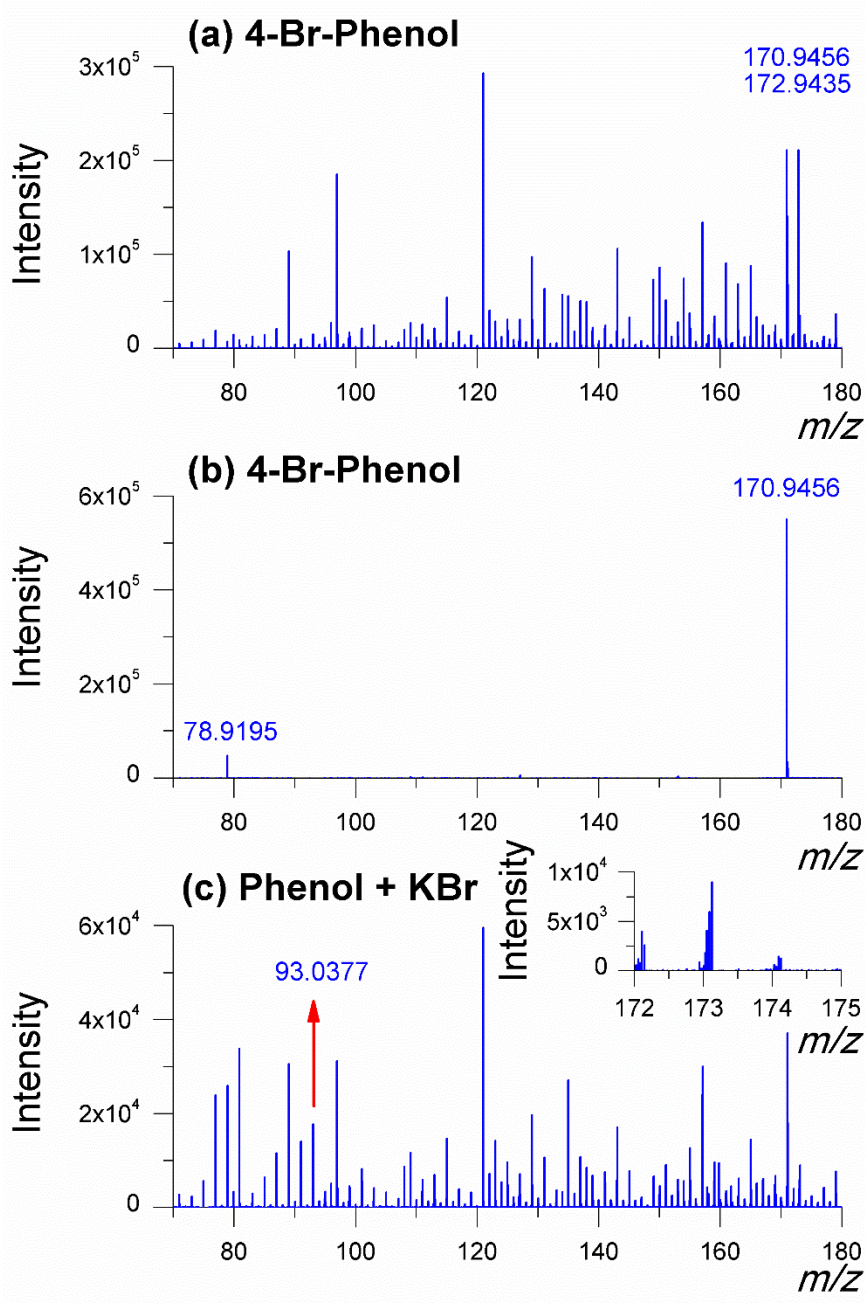

Figure S8: (a) Principal Component Analysis score plot on SML samples that were analyzed with both TM-DART-QTOF-MS and lab-to-the-field approach; samples that exhibited particle formation are shown with green squares, and samples that did not exhibit particle formation are shown with red squares. (b) Loadings plot associated to PC2 (B).

(a)

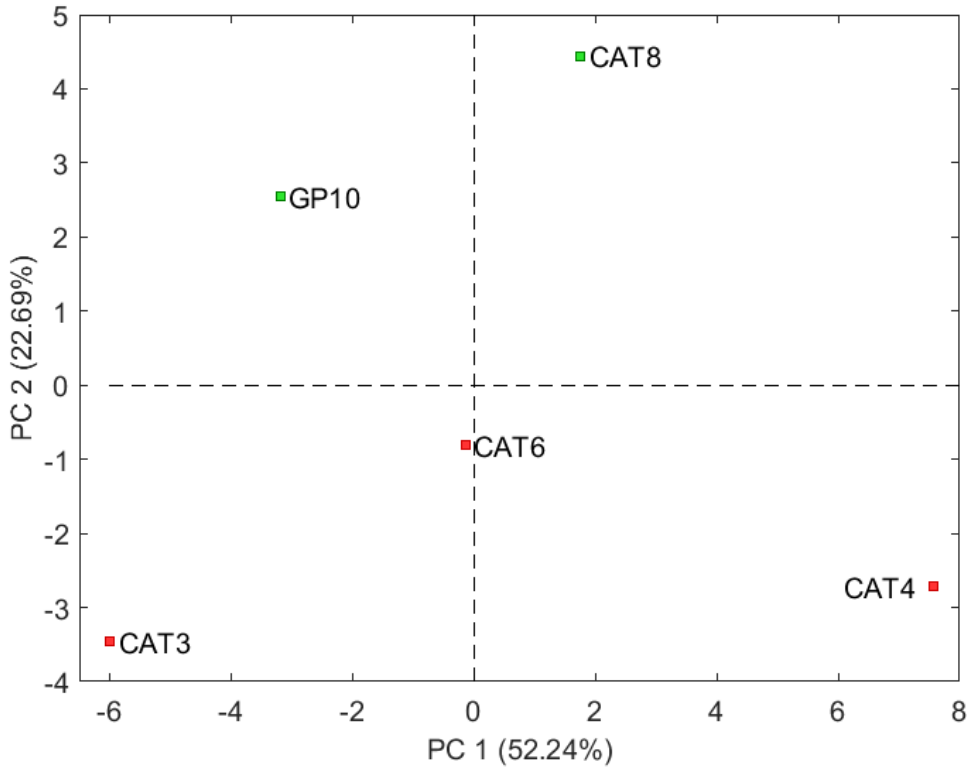

(b)

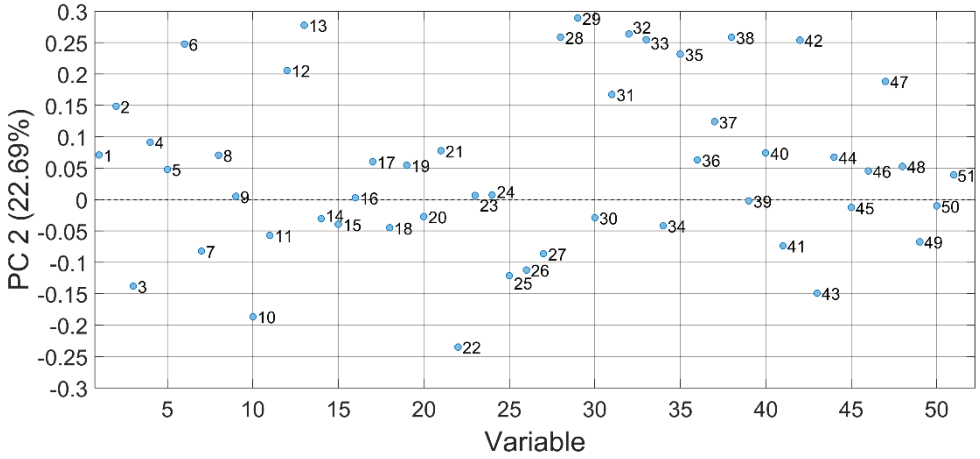

Supporting References

Carpenter, L. J., Fleming, Z. L., Read, K. A., Lee, J. D., Moller, S. J., Hopkins, J. R., Purvis, R. M., Lewis, A. C., Müller, K., Heinold, B., Herrmann, H., Fomba, K. W., Pinxteren, D. van, Müller, C., Tegen, I., Wiedensohler, A., Müller, T., Niedermeier, N., Achterberg, E. P., Patey, M. D., Kozlova, E. A., Heimann, M., Heard, D. E., Plane, J. M. C., Mahajan, A., Oetjen, H., Ingham, T., Stone, D., Whalley, L. K., Evans, M. J., Pilling, M. J., Leigh, R. J., Monks, P. S., Karunaharan, A., Vaughan, S., Arnold, S. R., Tschritter, J., Pöhler, D., Frieß, U., Holla, R., Mendes, L. M., Lopez, H., Faria, B., Manning, A. J. and Wallace, D. W. R.: Seasonal characteristics of tropical marine boundary layer air measured at the Cape Verde Atmospheric Observatory, J. Atmospheric Chem., 67(2–3), 87–140, doi:10.1007/s10874-011-9206-1, 2010.

Kang, E., Toohey, D. W. and Brune, W. H.: Dependence of SOA oxidation on organic aerosol mass concentration and OH exposure: experimental PAM chamber studies, Atmospheric Chem. Phys., 11(4), 1837–1852, doi:https://doi.org/10.5194/acp-11-1837-2011, 2011.

Li, R., Palm, B. B., Ortega, A. M., Hlywiak, J., Hu, W., Peng, Z., Day, D. A., Knote, C., Brune, W. H., de Gouw, J. A. and Jimenez, J. L.: Modeling the Radical Chemistry in an Oxidation Flow Reactor: Radical Formation and Recycling, Sensitivities, and the OH Exposure Estimation Equation, J. Phys. Chem. A, 119(19), 4418–4432, doi:10.1021/jp509534k, 2015.

Palm, B. B., Campuzano-Jost, P., Ortega, A. M., Day, D. A., Kaser, L., Jud, W., Karl, T., Hansel, A., Hunter, J. F., Cross, E. S., Kroll, J. H., Peng, Z., Brune, W. H. and Jimenez, J. L.: In situ secondary organic aerosol formation from ambient pine forest air using an oxidation flow reactor, Atmospheric Chem. Phys., 16(5), 2943–2970, doi:https://doi.org/10.5194/acp-16-2943-2016, 2016.

Peng, Z., Day, D. A., Stark, H., Li, R., Lee-Taylor, J., Palm, B. B., Brune, W. H. and Jimenez, J. L.: HO_x radical chemistry in oxidation flow reactors with low-pressure mercury lamps systematically examined by modeling, Atmospheric Meas. Tech., 8(11), 4863–4890, doi:https://doi.org/10.5194/amt-8-4863-2015, 2015.

Saukko, E., Lambe, A. T., Massoli, P., Koop, T., Wright, J. P., Croasdale, D. R., Pedernera, D. A., Onasch, T. B., Laaksonen, A., Davidovits, P., Worsnop, D. R. and Virtanen, A.: Humidity-dependent phase state of SOA particles from biogenic and anthropogenic precursors, Atmospheric Chem. Phys., 12(16), 7517–7529, doi:https://doi.org/10.5194/acp-12-7517-2012, 2012.